1

APPLICATIONS OF HIGH-RESOLUTION GIGAPAN IMAGERY IN MAPPING FRACTURE SYSTEMS: AN EXAMPLE FROM THE ADIRONDACK BASEMENT MASSIF, NEW YORK

RACHEL J. LEE,[1] BRANDON MAXWELL,[1] DAVID W. VALENTINO,[1] AND JOSHUA D. VALENTINO[2]

1. Department of Atmospheric and Geological Sciences, State University of New York at Oswego, 394 Shineman Science Center, Oswego, NY 13126; (315) 312-3065

2. GeoConcepts Engineering Inc., 19955 Highland Vista Dr., STE. 170, Ashburn, VA 20147

KEYWORDS:

GigaPan, Fault Density, Piseco Lake shear zone

ABSTRACT

The Precambrian basement and overlying rocks that comprise the Adirondack massif have experienced significant brittle deformation with uplift over time. This has produced an extensive system of faults and fractures, which trends generally North-Northeast (N-NE) throughout the massif. The fault and fracture system is well-exposed at numerous outcrops, which has proven advantageous to characterizing it. In this study, fault density analysis was conducted on 12 well-exposed outcrops within the Piseco Lake shear zone in the southern Adirondacks. A combination of orientation measurements and high-resolution GigaPan panoramic imagery were collected at each outcrop, and together these data were used to generate fault density contour maps of the outcrops. The fault density and orientation data has been integrated into a new Google Earth-based interactive structural field map of the Adirondacks, which can be further built upon by the authors (and others) as additional field campaigns are completed. This study has successfully served as a proof-of-concept for the imaging and contouring method, and has demonstrated its efficacy to geological research. Characterizing the quantity and spatial distribution of bedrock joints and fractures has important implications in geological fields such as hydrogeology, resource exploration, geo-hazard assessment, and geo-engineering.

INTRODUCTION

Over the past several decades, geologic field mapping and field data collection has progressively entered the digital age. The merging of traditional field methods (physical orientation measurements using a Brunton compass, on-site mapping of fractures and bedding relationships by hand, etc.) with modern mapping and measurement technologies is becoming more commonplace, especially as technology improves and becomes increasingly user-friendly. Maps and spatial data can now be quickly and easily presented, shared and interpreted in 2D and 3D using programs such as ArcGIS, Google Earth, and Structure from Motion; and using instruments such as LIDAR, drones, terrestrial laser scanners, and GigaPan.

The GigaPan instrument was developed in 2008 as a collaborative project among Carnegie Mellon University, NASA Ames Research Center, and Google. A variation of this instrument is currently part of the Mars Curiosity Rover payload and captures high-definition panoramas of Mars. For the past ten years, GigaPan technology has been progressively utilized for multi-scale geological outcrop visualization, largely for educational purposes (Schoen and Stevenson 2010, Steullet et al. 2010, Stimpson et al. 2010, Bentley et al. 2012, Benton et al. 2014, Pitts et al. 2014, Rohrback et al. 2014). Using GigaPan to create virtual field trips of geological areas on Earth (Kairies-Beatty and Beatty 2009, Lea and Urquhart 2011, Dordevik et al. 2015, Oakley et al. 2017) and on Mars (Johnson and Piatek 2014) has also gained popularity, greatly improving the overall accessibility of geological information to the public.

The use of GigaPan in qualitative and quantitative geological research has also grown tremendously in recent years. For example, high-resolution imagery generated from GigaPan has been used to study carbonate reservoirs (Qaio et al. 2015), fracture systems (Mastouri et al. 2015), dune geomorphology (Chan and Bruhn 2014, VanEyl-Godin and VanZytfeld 2015), magmatic and volcanological features (Gajos et al. 2013, Weinell et al. 2017, glacial geology (Wizevich and Piatek 2013), erosion rates of geological materials (Cathey et al. 2012, Hough et al. 2018), metamorphic mineralogy in the Adirondacks (Bernard et al. 2018, Botting et al. 2018), stratigraphic relationships (e.g., Nieto et al. 2013), and the geology of the Canadian Rockies (Bentley and Barth 2014). The technology also has seen increasing use in the areas of entomology (Bertone et al. 2012), archeology (Sisk 2010), time-lapse photography (Sargent et al. 2010), and is an integral part of NASA's robotic planetary analog field testing campaigns (Lee et al. 2010, 2013). Using the bedrock of the southern Adirondacks as a natural laboratory, the objectives of this investigation were 1) to integrate traditional structural geology field methods with GigaPan imaging techniques to characterize the geometry and density of fracture systems, fracture zones and exposed faults and 2) to use these data to develop a new Google Earth-based interactive structural field map.

GEOLOGIC SETTING

The Adirondack Mountains constitute an elongated topographic dome approximately 200 kilometers (km) in diameter. The region is thought to have been steadily uplifting for the past 20 million years; however, it has been proposed that uplift has been occurring since the Jurassic period (Roden-Tice et al. 2000). Although proximal to the Appalachians, the Adirondack massif is not geologically related to them. Rather, the massif is underlain by Precambrian Shield which extends from Canada through the St. Lawrence River valley and into the Adirondack region. Much of the Adirondack mineralogy and lithologies overlying this Precambrian basement rock formed during the Mesoproterozoic Grenville orogeny (~1 Ga [giga-annum; billion years]), and subsequent orogenic events (Chiarenzelli and Selleck 2016).

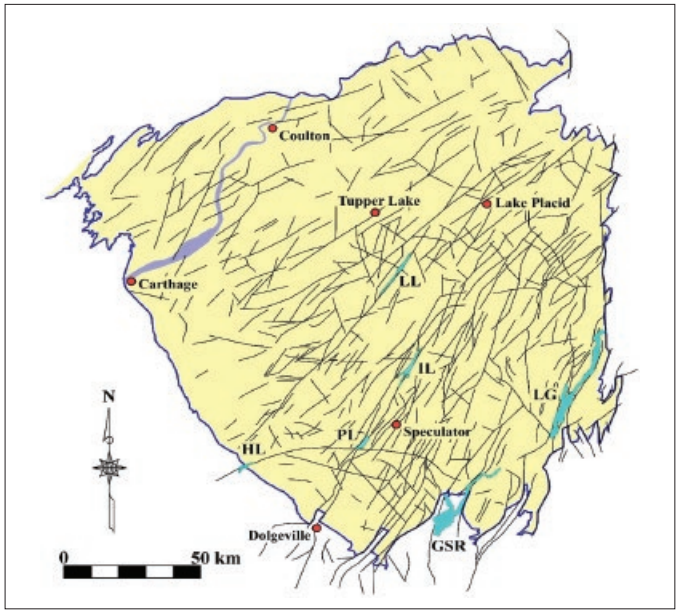

Figure 1: *Map of the Adirondack region (modified from Isachsen and McKendree 1977) showing prominent lineaments and faults, represented by black lines. Faults and lineaments predominantly trend in the N-NE direction, with minor lineament sets trending east-northeast, east-west, and north-south.*

Both the basement and overlying rocks that comprise the Adirondacks have experienced significant brittle deformation with uplift over time, producing extensive regional faults and fracture zones which trend generally N-NE throughout the Adirondack dome (Figure 1) (Isachsen 1981, Valentino et al. 2011). The majority of these structures lack evidence of recent displacement and are believed to represent tensional features formed during post-orogenic denudation (Isachsen et al. 1983), although it has been proposed that fault systems in the northwestern Adirondacks in particular continue to be affected by neo-tectonic and low-level seismic activity (Isachsen 1981; Barosh 1986, 1990, 1992; Daneshfar and Benn 2002; Wallach 2002). It is possible that regional uplift is responsible for producing many of the fault systems within the Adirondacks, although some researchers (e.g., Jacobi 2002) hypothesize that much of the faulting entirely pre-dates dome formation. For example, samples of apatite fission tracks collected from blocks of Adirondack rocks have shown that N-NE trending normal faults are actually 80-100 Ma (mega-annum; million years) older than the W-NW fault systems (Roden-Tice et al. 2000). This supports the theory that different localities of the Adirondack dome have uplifted and unroofed at various rates, which has contributed to the structural complexity within the dome.

Overall, the rate of uplift thus far exceeds the rate of denudation, which has allowed for the structurally-deformed Precambrian basement rock to be well-exposed throughout the region. Faulting and fracture intensification domains seen at both the surface and at depth correspond with the rising basement rock, and this mechanism provides the stress needed for widespread lineaments to form (Jacobi 2002). The underlying cause for uplift—and the timing—remains a matter of debate. The most widely-accepted theory involves purported regional volcanic hot-spot activity and associated mantle buoyancy (Yang and Gao 2018). Portions of the dome have undergone uplift in a more segmented style, which has been attributed to rift faulting in the area in association with the formation of the Iapetus Ocean in the Neoproterozoic (Roden-Tice et al. 2000, Jacobi and Mitchel 2002). In other areas, uplift is more differential in nature, likely due to the reactivation of faults (Roden-Tice et al. 2000, Roden-Tice and Tice 2009).

The Adirondack fault and fracture system is particularly well-exposed at numerous outcrops throughout the region, which has proven advantageous for studying and observing it directly at the surface. The system manifests as dominantly NE-trending lineaments, which are cut by other minor lineament sets trending E-NE, E-W, and N-S (Valentino et al. 2012). Despite the well-exposed outcrops available for study, the overall complexity of the Adirondack fault and fracture system, coupled with the often dense vegetative cover throughout most the region, makes observation and characterization of the large-scale structural relationships quite challenging.

FRACTURE DENSITY ANALYSIS

Outcrops that underwent fracture density analysis in this study were located along the Prospect Fault and the Piseco Lake shear zone. Although many more fracture-dense outcrops of various lithologies exist in the Adirondacks than those studied here, outcrops at which lighting was too poor to acquire useable imagery or to perform an accurate fracture count, or at which dominant fracture sets were completely invisible due to very dense vegetation cover, could not be included in this study.

A GigaPan instrument was used to collect an overlapping grid of images at each imaged outcrop. A GigaPan is a portable, tripod-mounted robotic instrument that houses a DSLR camera and allows for the camera to take hundreds of individual photos at high resolution. Individual images are imported into GigaPan Stitch image processing software, which organizes the images into a grid and then stitches them together to create a single giga-pixel, "zoomable" panoramic image (Figure 2). These panoramic images provide an effective means of analyzing multi-scale geologic features over wide areal extents, as they can be zoomed into and panned in various directions.

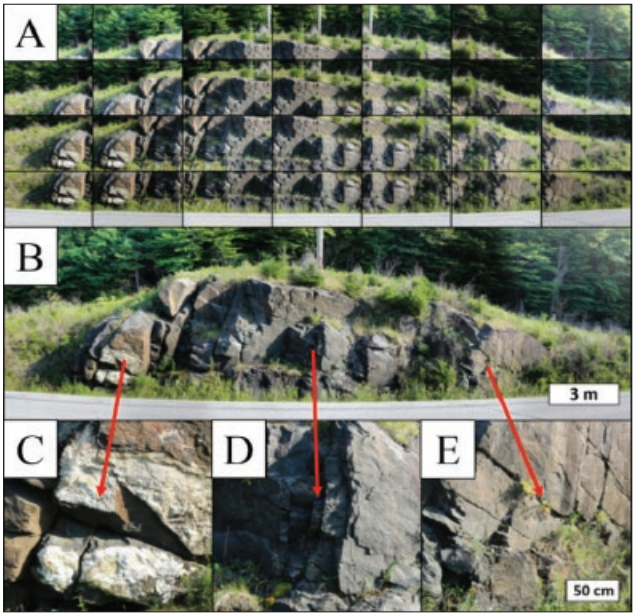

Figure 2: *(A) The GigaPan captures images in a grid pattern, the size and shape of which is established by the user. Twenty-eight individual photographs were taken of this outcrop, with a 35 percent image overlap. Each image was acquired with the camera at full zoom to capture as much detail as possible. (B) Images are stitched together to create a single high-resolution image. Zooming in to various areas (C–E) allows the user to easily inspect multi-scale features and composition. Red arrows denote areas of the outcrop that appear in images C-E.*

Additionally, the height and width of the outcrop, as well as the dimensions of notable features, were measured in the field to provide an accurate scale for the imagery. Where features were inaccessible, a laser rangefinder was used to measure height and thickness of features. These measurements provided a quantitative scale for the panoramic images. Orientation measurements (strike and dip) were also collected for fractures and faults on each outcrop, and these data were used to characterize the attitude of the brittle structures within the outcrops. Outcrop orientation measurements made in this study were corroborated by lineament orientations on existing maps (Isachsen and McKendree 1977, Valentino et al. 2012) and by orientation measurements of the area previously collected by David Valentino (Figure 3).

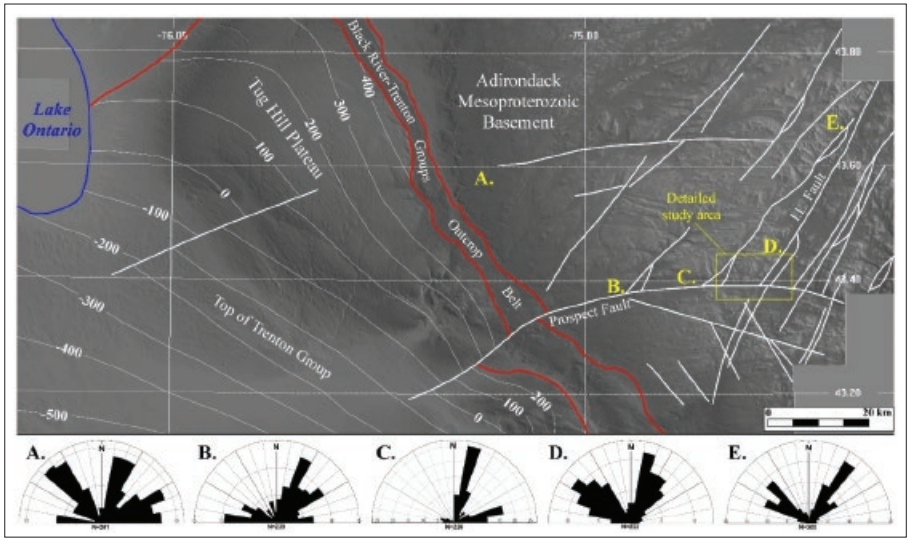

Figure 3: *Digital elevation model and structure contour map of the Tug Hill plateau, Trenton Group, and Prospect Fault (Southern Adirondacks). The orientation diagrams shown here were created from measurements collected at points A-E on the map, and clearly show the dominant N-NE strike of the faults and fracture systems in this area. These measurements are consistent with the orientation measurements acquired for this study (as seen in the Appendix). The study area presented here is marked by the yellow square on the map.*

GigaPan imagery and field measurements were then used collectively to create a fracture density map for each outcrop. On the GigaPan image, the number of fractures per meter that were perpendicular to the strike of the fracture was quantified. Two different techniques were used for this analysis. In the random interval sampling technique, only those fracture sets identified on the image as trending perpendicular to the face of the outcrop (parallel to the direction of the GigaPan image) were analyzed (Figure 4). The density (inverse of fracture spacing) of these fracture sets was then estimated by counting and averaging the number of fractures occurring within 1-meter areas chosen at random intervals along the outcrop.

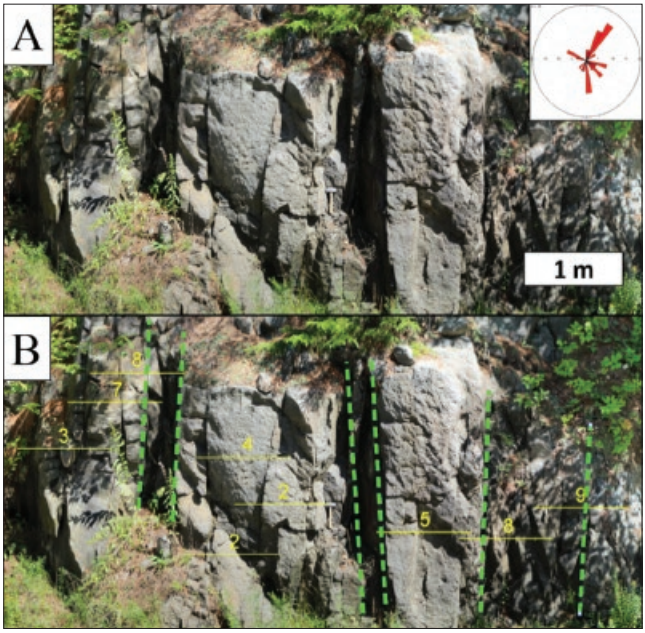

Figure 4: *The random interval sampling technique for determining fracture density. (A) Strike and dip measurements of fracture surfaces were taken at each outcrop and dominant fracture orientations were noted. Fracture sets trending perpendicular to the face of the outcrop (parallel to the direction of the image) were used to estimate fracture density. (B) Fracture density (fractures/meter) was estimated by counting and averaging the number of fractures that occur within one meter at random intervals along the outcrop, in a direction normal to the fracture set. Zones of high fracture density (green dashed lines) were documented but were not averaged into the sites' overall densities.*

A more rigorous technique for quantifying fracture density, which garnered greater success, involved using Canvas X software to superimpose a scalable square grid onto each panorama. A 1 meter x 1 meter (m) grid was applied to outcrops with larger extents, and a 0.5 m x 0.5 m grid was used for smaller outcrops. The number of fractures occurring in each grid square, regardless of their orientation, was noted. Each central node located at the intersection four individual grid squares yielded the average fracture density per $4m^2$ (Figure 5).

There are no nodes on the edge of the image grid; thus, an average fracture density could not be calculated at the edges using this method. To resolve this issue, a border was created around each outcrop panorama so that the edges of the image were not contoured. Otherwise, values of 0 would be assumed for the edge of the outcrop and the density contour lines produced would be inaccurate. Borders were created in the same fashion as a grid of XY data, where the X values represented the horizontal grid lines and Y values represented the vertical lines, with a value of (0,0) at the intersection of the X and Y axis. After central nodes were derived and averaged on the scaled grid, the statistical program *Surfer 11* was used to create the fracture density contour maps for the outcrops. Data for each outcrop were first organized into an Excel spreadsheet in an XYZ format where X represented horizontal meters, Y represented vertical meters, and Z represented the centralized node value of fracture density derived from the grid. These data were used in *Surfer 11* to create a fracture density contour map for each outcrop, which was then superimposed on the original GigaPan image (Figure 6).

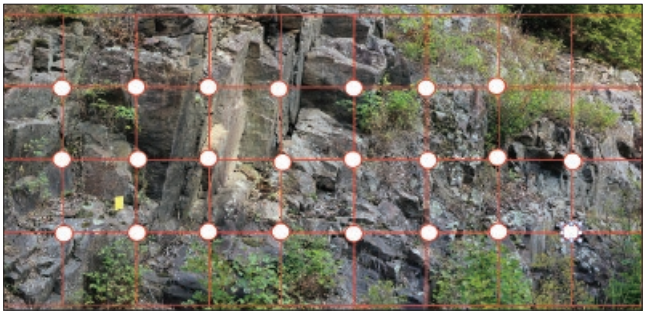

Figure 5: *The scalable square grid method for determining fracture density. A scaled grid (red lines) was applied to each outcrop (Site 3 shown here), and the number of fractures occurring in each grid square, regardless of their orientation, was noted. Each central node at the intersection four grid squares (white circles) yielded the average fracture density per 4 m².*

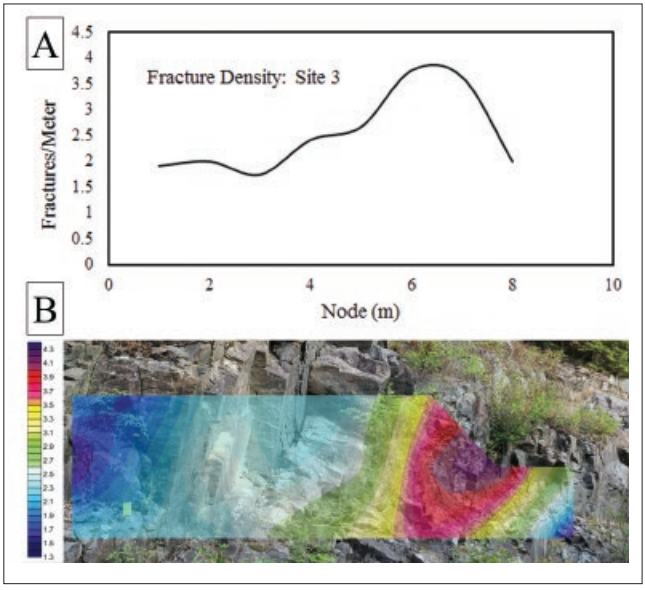

Figure 6: *(A) Graph of fracture density/meter at each grid node for Site 3. These data were incorporated into Surfer 11 to create a density contour map for the outcrop. (B) The resulting contour map of fracture density for Site 3. Lower fracture density areas (blues) indicate more competent rock, whereas higher fracture density areas (reds) indicate less competent rock and supplement the "background" fracture density of dominant fracture sets. This contouring process was repeated for all 12 outcrops in the study.*

Despite limiting the study to well-exposed outcrops with easily observable fractures, several outcrops in this study had small areas of significant foliage present, but were still able to be imaged. In this case, a specialized border was created so that only bare rock faces where fractures could be easily seen were contoured, and foliage was eliminated from the analysis (Figure 7). Some outcrops were comprised of a number of distinct lithotectonic facies and often exhibited fractures with no clear orientation. In this case, it was determined that lower fracture density areas on the contour maps are representative of more competent rock, whereas higher fracture density areas denote relatively less competent rock. (*See Appendix for the resulting contour maps for all 12 outcrops analyzed in this study.*)

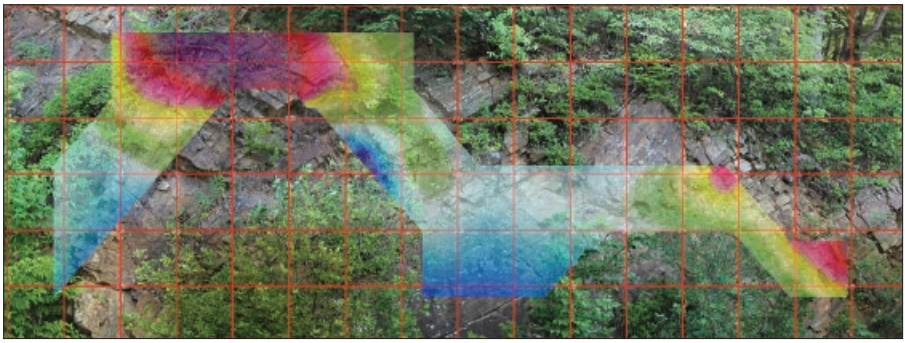

Figure 7: *In an effort to only account for exposed rock surfaces when counting fractures, specialized borders were created on the images of outcrops which contained a higher density of foliage. The resulting fracture density contour map was then restricted to the specialized border. In this fracture density contour map, purple contours denote highest fracture density and blue contours denote the lowest fracture density.*

Rose diagrams generated from orientation measurements collected in the field, along with the panoramic imagery and available joint density data, were incorporated into a new Google Earth-based interactive field map of the Adirondacks. On this map, the location of each outcrop included in this study is marked. When a symbol is selected on the map, a thumbnail of the associated GigaPan image acquired at that outcrop is displayed, along with the accompanying orientation diagram and fault density contour map (Figure 8). This map is an on-going venture and will be further developed into a digital field guide to fault and fracture systems throughout the Adirondacks as additional data is collected from outcrops in future field campaigns. (Access to the database of the full resolution GigaPan imagery, as well as associated fracture density contour maps, is available upon request.)

DISCUSSION

Fault density analyses and fracture orientation measurements were completed for a set of twelve outcrops located along the Prospect Fault and within the Piseco Lake shear zone (PLSZ). The PLSZ cross-cuts the general NE-SW trending fractures and lineaments which were produced during earlier stages of uplift in the Adirondacks, and the area has undergone intense deformation and fracturing in association with the Prospect Fault, producing areas of high fracture density (Figure 9). The high intensification of fractures in the aforementioned areas, combined with generally low vegetative cover, was conducive to mapping and analysis. Zones with fracture density of ≥10 fractures/meter were observed at several sites, almost always in outcrops oriented perpendicular to the major NE- SW fracture system. Conversely, fracture density appears to be lowest at those outcrops which trend parallel to the NE-SW fracture system. This observation is supported by the Isachsen and McKendree (1977) and Valentino et al. (2012) lineament maps. From this, it can be assumed that larger-scale fracture zones may be reasonably inferred from the outcrop-scale GigaPan imagery and fracture density analysis presented here.

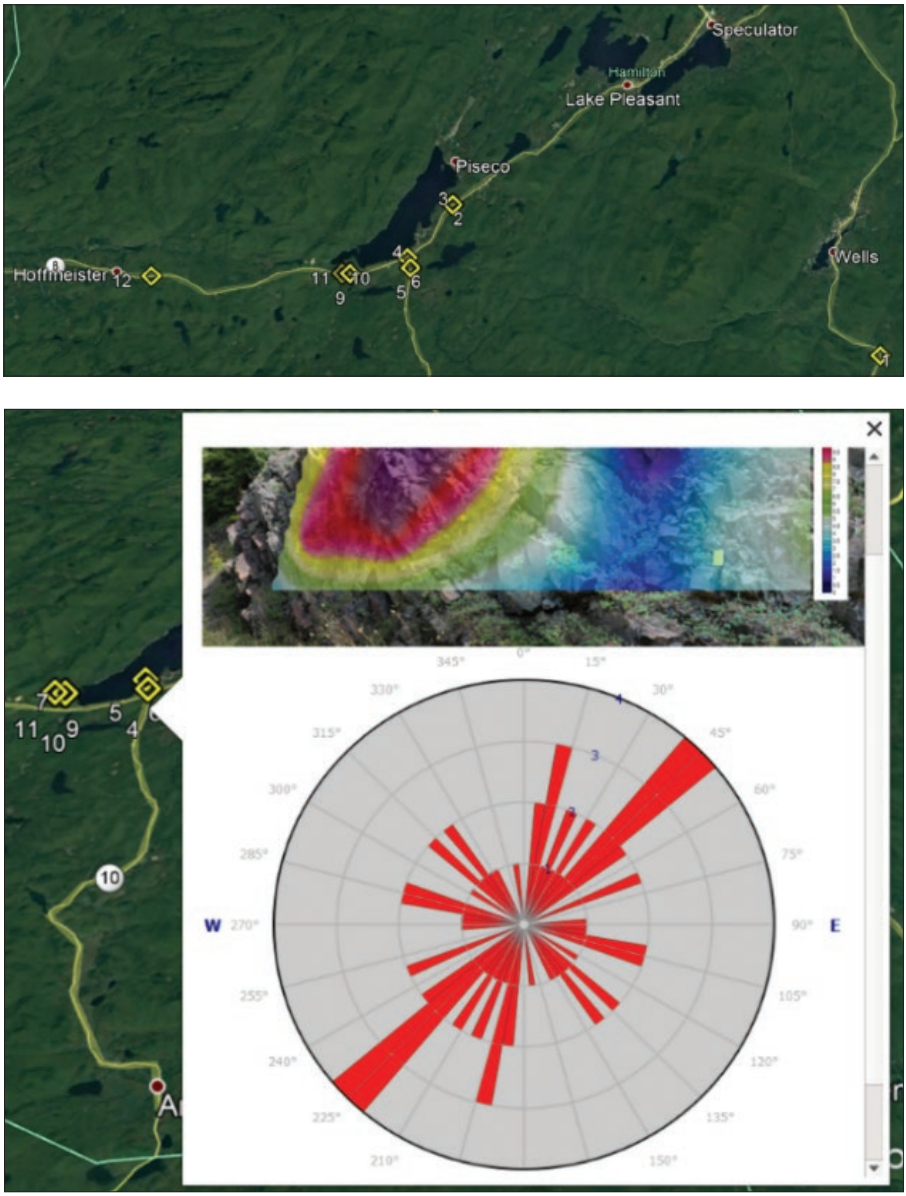

Figure 8: *The locations of all 12 outcrop sites in this study are marked on the Google Earth map (top). Users can examine a site by selecting the appropriate yellow symbol on the map. Once a symbol is selected, the panoramic image and fault density map of the outcrop are shown, as well as the accompanying rose diagram. The database of full-resolution versions of all imagery, as well as fracture density contour maps, are downloadable by the user.*

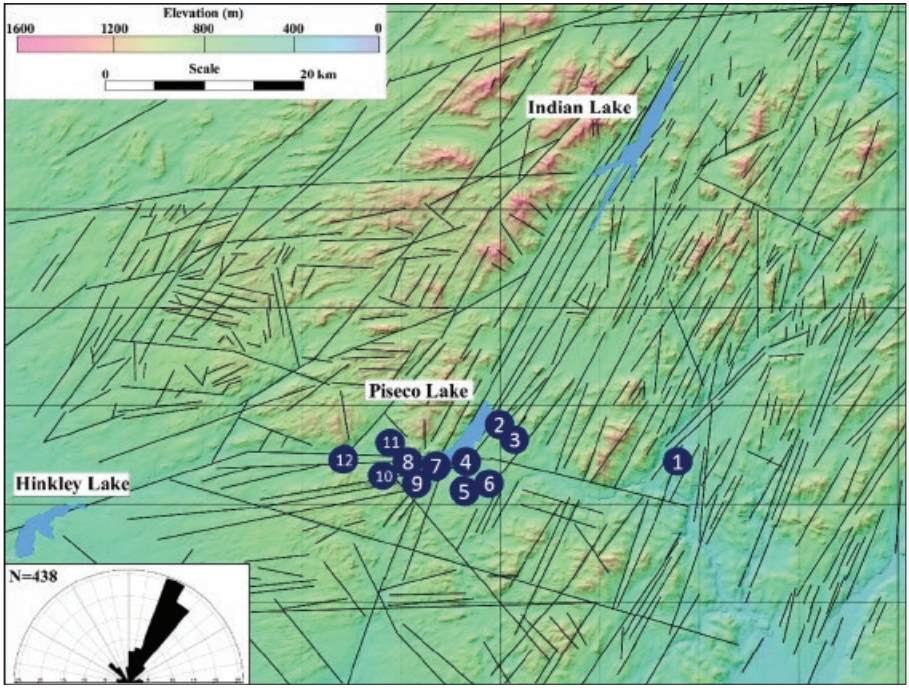

Figure 9: *DEM lineament model (Valentino et al. 2012) showing structural trends and fracture intensification zones within the southern Adirondack region. Orientation diagram shows the general N-NE trend of lineaments in this region. Numbered blue dots denote the site locations of outcrops analyzed in this study. Much of the faulting and fracturing in the Piseco Lake Shear Zone is due to activity along the Prospect Fault, which extends in an E-W direction through the Piseco Lake region and directly through most of the outcrops presented in this study.*

The contouring technique has proven successful in efficiently and accurately characterizing localized fault density and orientation, and findings correspond with existing lineament maps. However, there are several limitations inherent in the technique that merit discussion. The presence of vegetation throughout the Adirondack region, much of it year-round, hinders the ability to directly observe the fracture systems at a larger, regional scale. Lidar overflights of the area are helpful for resolving fractures beneath vegetation but are cost-prohibitive, and they are limited in availability. Due to this, most structural studies are currently restricted to those areas with accessible outcrops that contain well-exposed fracture systems, and this introduces some sampling bias in terms of the type and amount of fracture information available in a given area. To minimize this bias, orientation measurements were still collected at outcrops that were fracture-dense but somewhat heavily vegetated, where imagery could not be successfully acquired. Despite this bias, the method does provide a means for effectively mapping the fracture pattern and density within smaller regions. Since it allows for interpretation throughout differing lithologies (where fracture density serves as a proxy for unit competence), this GigaPan-based fracture density analysis technique has additional potential uses, including mapping groundwater flow and finding potential locations of local to regional-scale petroleum, mineral, and ore resources.

The GigaPan instrument was somewhat limited in this study by its orientation to the outcrop. If it is oriented at any angle other than perpendicular to the dominant fracture set, or if the panoramic image covers too large of an extent, the edges of the panoramic image can become deformed, making fracture counting more problematic at the edges. The number of fractures per meter could be miscounted towards the edges of an image, as the edges are not at a true meter-scale and do not accommodate the fracture-count grid as accurately as the rest of the image. One method for solving this problem is to collect several square-shaped panoramic images of an outcrop which have an overlap with one another. These panoramas can then be stitched together to create a continuous panoramic image with minimal to no edge distortion. This method was employed for several of the outcrops imaged toward the end of the study period. This panoramic imagery better accommodated the 1-meter grid and helped improve accuracy of fracture counting at the image edges. In the next series of field campaigns planned for this project, imagery of outcrops will be re-collected in this manner in an effort to improve the accuracy of the fracture counting and the interactive map. Small-scale fractures due to spalling and other non-tectonic processes (e.g., road blasting) may also sometimes resemble significant fractures in the outcrop depending on the orientation and lighting of the image. Although large-scale human-induced fracturing was ignored in the fracture count where it was visible to the eye, smaller- scale features may have been counted, resulting in some miscounts of fracture intensification in various locations at an outcrop.

Despite the high level of detail in each image, shadows cast by vegetation and other features in several cases proved to be indistinguishable from small fractures. Capturing images at varying angles, and at varying times of the day (or during cloudy days), would help eliminate the majority of shadows. Furthermore, panoramic imagery captured at varying angles relative to outcrops allows for inexpensive 3D models of outcrops to be generated using software such as AGI PhotoScan. This 3D modeling technique is currently being tested on imagery from several southern Adirondacks outcrops as part of a different project (Karimi and Lee 2018). The technique will be applied to additional imagery collected during future field campaigns for fracture density analysis, and will further improve the fracture density mapping technique and provide upgraded data to the interactive map. Ultimately, this map will provide Adirondacks researchers and the public with an open-source, user-friendly database of imaged and modeled outcrops within the Adirondacks.

CONCLUSION

Uplift and deformation within the Adirondack massif over the last 20 million years has extensively deformed and faulted the region, which has resulted in a high density of fractures dominantly in the NE-SW and E-W directions, depending on locality. Traditional field techniques and GigaPan panoramic imagery were utilized for both qualitative and quantitative analysis of a series of fault-dense outcrops within the southern Adirondacks. Fracture density contour maps were created and superimposed on the panoramic imagery in order to quantify fracture presence and density within outcrops. The structural information obtained in this study corroborates previous field work and mapping by Isachsen and McKendree (1977) and others in the region. The use of the GigaPan instrument has expedited the collection of visual information at the outcrop scale reducing time spent in the field and has allowed for detailed mapping of outcrop features and efficient collection of fracture density data. A Google Earth interactive field map containing the data from this study has the potential to grow into a shared interactive digital library of geological sites throughout the Adirondack region on which the authors and others can build.

FOR THE FOLLOWING 12 FIGURES: Blue, green and purple colors (and associated numerical values) denote relatively lower fracture densities, whereas yellows, oranges, and reds denote relatively higher fracture densities. Rose diagrams indicate the orientation of the dominant fracture sets at each outcrop.

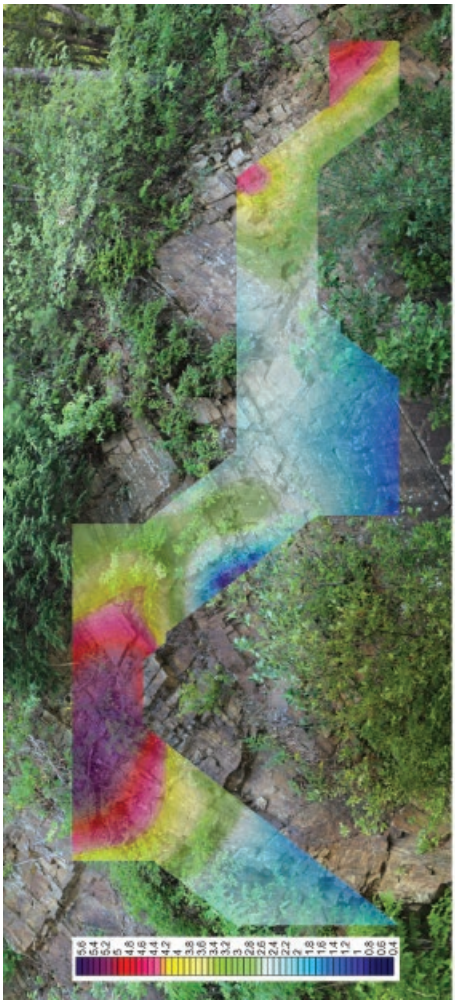

Site 1
Location: N43° 20'58.0" W74° 15;43.0"
Avg. Height: 5.7m **Avg. Width:** N/A

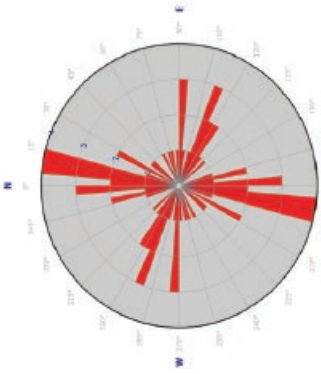

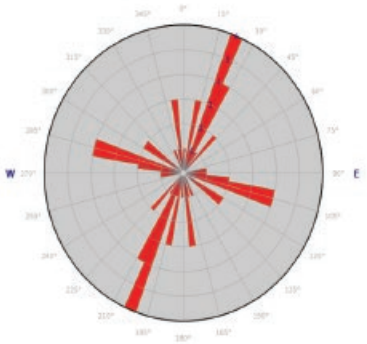

Site 2

Location: N43°25.114' W074°31.042'

Avg. Height: 5.6m **Avg. Width:** (N/A)

Site 3
Location: N43°25.114' W74° 31.042'
Avg. Height: 54m **Avg. Width:** N/A

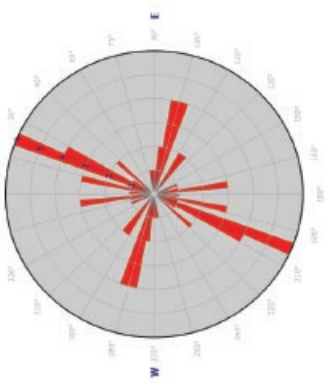

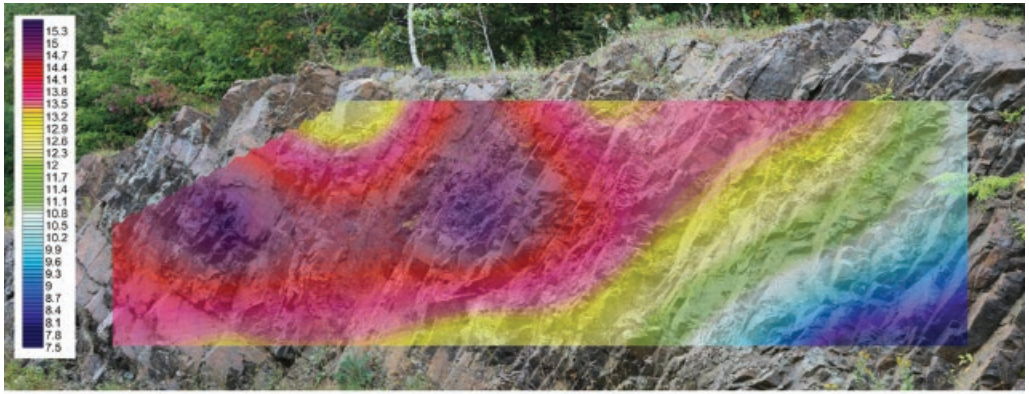

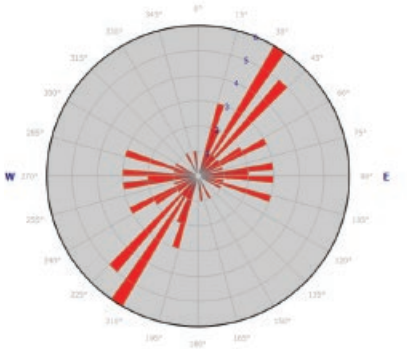

Site 4

Location: N43°23.718' W74°32.689'

Avg. Height: 3.825m **Avg. Width:** 86.7m

Site 5
Location: N43°23.446' W74°32.579'
Avg. Height: 3.97m **Avg. Width:** 62m

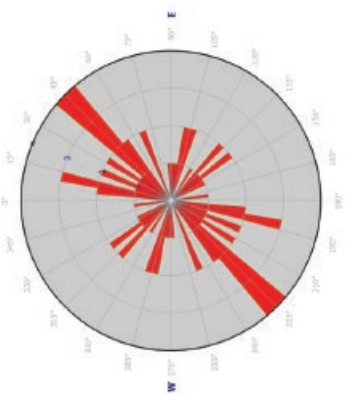

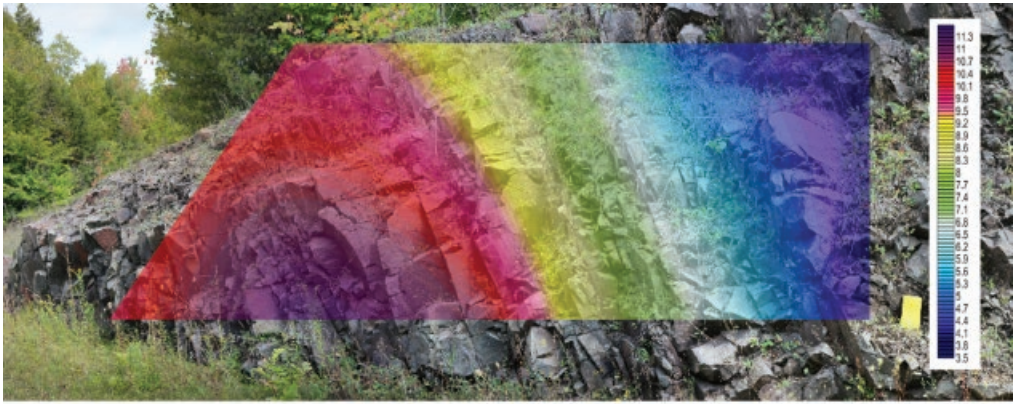

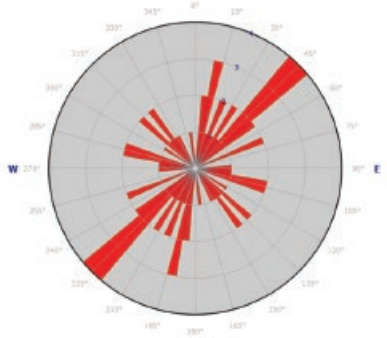

Site 6

Location: N43°23.446' W74°32.579'

Avg. Height: 3.97m **Avg. Width:** 62m

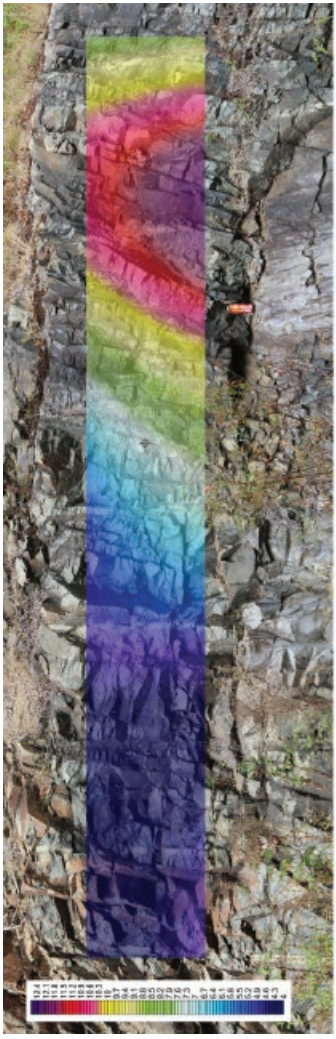

Site 7
Location: N43°23.322' W74°35.029'
Avg. Height: 4.21m **Avg. Width:** 83m

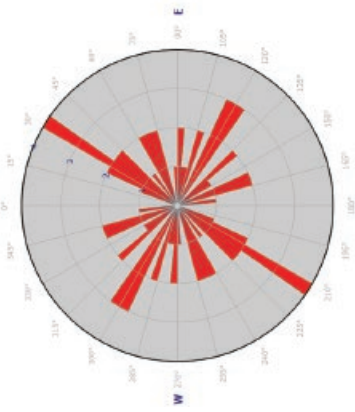

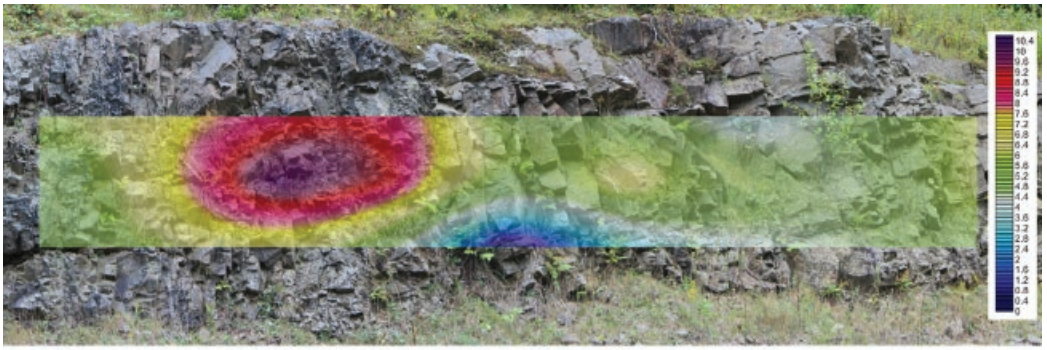

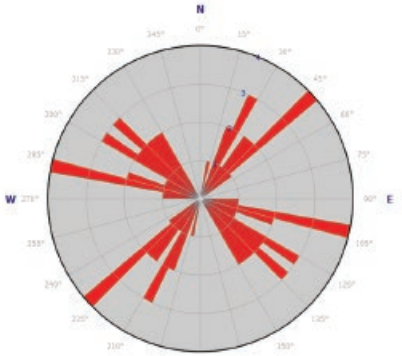

Site 8

Location: N43°23.313' W74°35.029'

Avg. Height: 2.08m **Avg. Width:** 33m

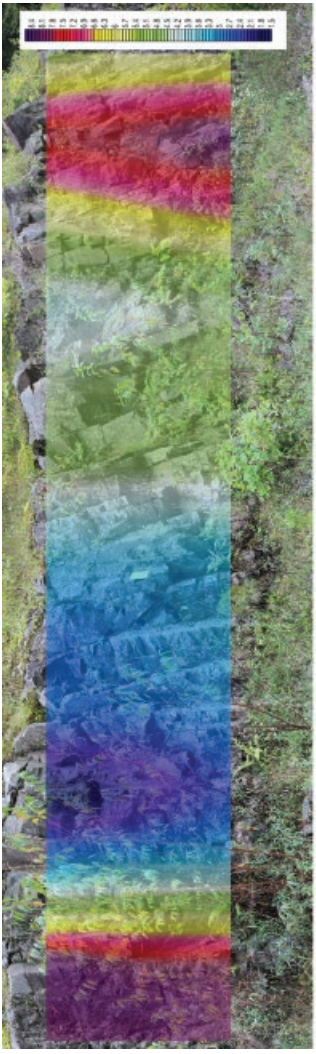

Site 9
Location: N43°23.308' W74°34.758'
Avg. Height: 3.29m **Avg. Width:** 208m

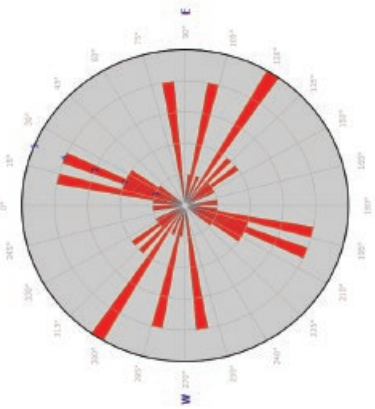

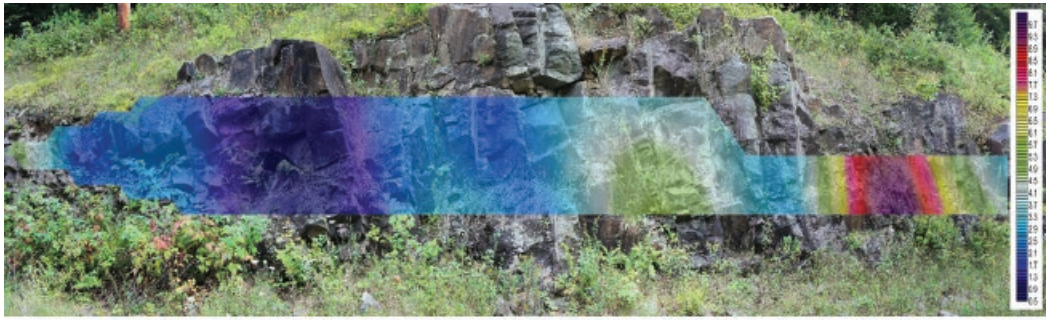

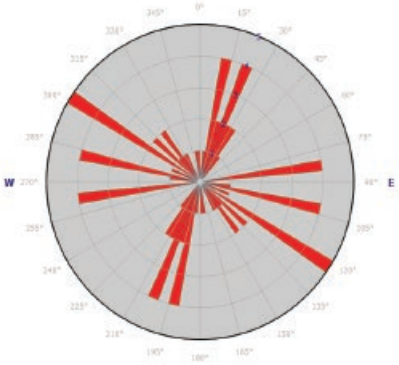

Site 10

Location: N43°23.308' W74°34.758'

Avg. Height: 3.29m **Avg. Width:** 208m

Site 11
Location: N43°23.309' W74°34.746'
Avg. Height: 6.58 **Avg. Width:** 156m

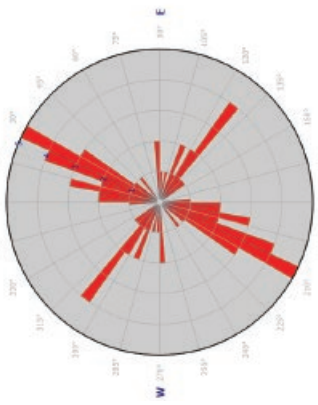

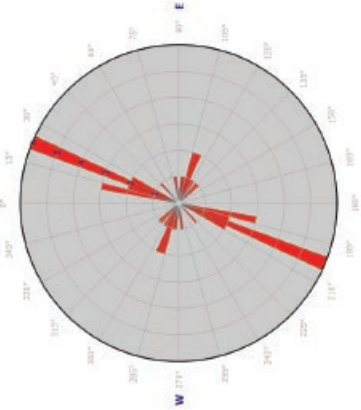

Site 12
Location: N43°23.287' W74°41.826'
Avg. Height: 1.91m **Avg. Width:** 74m

REFERENCES

Barosh, P.J. 1986. "Neotectonic movement, earthquakes and stress state in the eastern United States." *Tectonophysics* 132: 117-152.

Barosh, P. J. 1990. "Neotectonic movement and earthquake assessment in the Eastern United States." *Rev. Eng. Geo.* 8: 77-109.

Barosh, P.J. 1992. "Northwest-trending basement fracture zones in the Eastern United States and their role in controlling neotectonic movement and earthquakes." *Proceedings of the International Conference on Basement Tectonics, Canberra, Australia* 7: 409.

Bentley, C., J. Piatek, and R. Schott. 2012. "Zooming in on geology with GigaPans." *GSA Annual Meeting*, Charlotte, *NC USA, Abstract #91-2*.

Bentley, C. and A. Barth. 2014. "Telling the story of the Canadian Rockies via Google Earth." *GSA Annual Meeting, Vancouver, BC Canada, Abstract #93-1*.

Benton, J., R. Rohrback, and C. Bentley. 2014. "The 'M.A.G.I.C.'AL growth of an online GigaPan repository for geoscience education." *GSA Annual Meeting, Vancouver, BC Canada, Abstract #28-3*.

Bernard, C., D. Valentino, and R.J. Lee. 2018. "Multi-Scale mapping of the metamorphic mineralogy of Edwards, Trainwreck, Snake and DeKalb outcrops (Adirondack Region) using thermal infrared, SEM, XRD and petrographic techniques." *GSA Northeastern meeting, Burlington, VT USA, Abstract #54-2*.

Bertone, M.A., R.L. Blinn, T.M. Stanfield, K.J. Dew, and K.C. Seltmann. 2012. "Deans, A.R. Results and insight from the NSCU Insect Museum GigaPan project." *Zookeys* 209: 115-132.

Botting, O., R.J. Lee, and D. Valentino. 2018. "Multi-Scale mapping of the metamorphic mineralogy of Popple Hill, Steer's Head and Antwerp outcrops (Adirondack Region) using thermal infrared, SEM, XRD and petrographic techniques." *GSA Northeastern meeting, Burlington, VT USA, Abstract #54-9*.

Cathey, S. T.; Seymour, K.N.; Hein, N.P.; Bodenbender, B.E. Using GigaPan measurement of erosion pins to monitor surface changes in sand, *GSA Annual Meeting, 2012, Charlotte, NC USA, Abstract # 233-13*.

Chiarenzelli, J. and B. Selleck. 2016. "Bedrock geology of the Adirondacks."*Adirondack Journal of Environmental Studies* 21: 19-41.

Chan, M.A. and R.L. Bruhn. 2014. "Dynamic liquefaction of Jurassic sand dunes: processes, origins and implications." *Earth Surf. Proc. Land.* 39: 1478-1491.

Daneshfar, B. and K. Benn. 2002. "Spatial relationships between natural seismicity and faults, southeastern Ontario and north-central New York state" *Tectonophysics* 353: 31-44.

Dordevic, M., D. DePaor, S.J. Whitmeyer, C. Bentley, G. Whittecar, and C.K. Constants. 2015. "Learning about the Earth in an interactive Google Maps/Street View/Photo Sphere/Giga-Pan challenge – the magical geology mystery tour!" *GSA Northeastern Annual Meeting, Bretton Woods, NH USA, Abstract #6-9*.

Gajos, N., C.C. Lundstrom, and N. Huggett. 2013. "Illuminating magmatic features at Torres Del Paine using high resolution GigaPan photography." *GSA Annual Meeting, Denver, CO USA, Abstract #143-5*.

Hough, B., N. Torres, M. Kensell, J. Bullock, and R.J. Lee. 2018. "Can GigaPan images be used as an alternative to LIDAR to measure erosion rates?: An experiment on glacial till at Chimney Bluffs State Park, Huron, NY." *GSA Northeastern Annual Meeting, Burlington, VT USA, Abstract #54-5*.

Isachsen, Y.W. and W.G. McKendree. 1977. "Preliminary brittle structure map of New York." *NYS Museum Map and Chart Series 31, Scale 1:125,000*.

Isachsen, Y.W. 1981. "Contemporary doming of the Adirondack mountains: Further evidence from releveling." *J. Tectonophysics* 71: 95-96.

Isachsen, Y. W., E.P. Geraghty, and R.W. Wiener. 1983. "Fracture domains associated with a neotectonic, basement-cored dome: the Adirondack Mountains, New York." In Gabrielsen, R. H. et al., eds. 1983 *Proceedings for the Fourth International Conference on Basement Tectonics, International Basement Tectonics Association, Oslo, Norway,* pp. 287-306.

Jacobi, R. and C. Mitchell, C. 2002. "Geodynamical interpretation of a major unconformity in the Taconic Foredeep: slide scar or onlap unconformity?" *Phys. Chem. Earth* 27: 169-201.

Jacobi, Robert D. 2002. "Basement faults and seismicity in the Appalachian Basin of New York State." *Tectonophysics* 353: 75-113.

Johnson, J.M. and J.L. Piatek. 2014. "The GigaPan guide to Mars: Using a virtual field trip to compare Earth and Mars." *GSA Northeastern Annual Meeting, Lancaster, PA USA, Abstract #28-1*.

Kairies-Beatty. C. and W. Beatty. 2009. "GigaPan, Google Earth, and geomorphology at the Gettysburg battlefield: Creating virtual field experiences for undergraduate students." *GSA Annual Meeting, Portland, OR USA, Abstract #192-5*.

Karimi, B. and R.J. Lee. 2018. "Multi-scale fractal analysis of fractures within a granitoid outcrop near Piseco Lake, Adirondacks, using high-resolution SEM and GigaPan imagery." *GSA Northeastern Annual Meeting, Burlington, VT USA, Abstract #310379*.

Lea, P. and J. Urquhart. 2011. "Using GigaPans and field photographs to create virtual field trips as a learning project in an undergraduate introductory geology course." *GSA Northeastern and North-Central Annual Joint Meeting, Pittsburgh, PA USA, Abstract #67-4*.

Lee, S., T. Morse, and E. Park. 2010. "GigaPan Voyage for robotic reconnaissance." *Fine International Conference on Gigapixel Imaging for Science, Paper 9*.

Lee, S., D. Lees, T. Cohen, M. Allan, M. Deans, T. Morse, E. Park, and T. Smith. 2013. "Reusable science tools for analog exploration missions: xGDS web tools, VERVE, and GigaPan Voyage." *Acta Astronaut* 90(2): 268-288.

Mastouri, R., A. Guerin, R. Marchant, M-H Derron, A. Boulares, M. Lazzez, F. Marillier, M. Jaboyedoff, and S. Bouaziz. 2015. "Fracture analysis of an Eocene reservoir in Eastern Tunisia by coupling Terrestrial Laser Scanning with GigaPan Technology and seismic attribute." *EGU General Assembly Geophysical Research Abstracts* 17: 13175.

Nieto, J., E. Sanderson, J. Cancellare, and D.J. Caskey. 2013. "Building a 'geologic library' of the Major lithologic units in the El Paso area." *American Geophysical Union Fall Meeting, Abstract #ED41C-0756*.

Oakley, B.A., M.A. Manzi, B.J. Sumeersamauth, and S. Boyle. 2017. "The Block Island Bluff image project: Using Google Earth™, Spreadsheet Mapper, and Google Drive™ to build a database of spatially located field images of coastal bluffs." *Journal of Coastal Research, EGU General Assembly* 33(2): 463-467.

Pitts, A., C. Bentley, and R. Rohrback. 2014. "Using photogrammetry, GigaPans, and Google Earth to build virtual outcrops for geologic research and educational outreach." *GSA Annual Meeting, Abstract #28-2*.

Qiao, Z., A. Shen, J. Zheng, S. Chang, and Y. Chen. 2015. "Three-dimensional carbonate reservoir geomodeling based on the digital outcrop model." *Petroleum Exploration and Development* 42: 358-368.

Roden-Tice, M.K., S.J. Tice, and I.S. Schofield. 2000. "Evidence for differential unroofing in the Adirondack mountains, New York State, determined by apatite fission- track thermochronology." *J. Geol.* 108: 155-169.

Roden-Tice, M. and S. Tice. 2009. "Regional-scale mid-Jurassic to late Cretaceous unroofing from the Adirondack mountains through central New England based on apatite fission-track thermochronology." *Journal of Geology* 113: 535-552.

Rohrback, R., C. Bentley, A. Pitts, C. Johnson, and S. Adler. 2014. "Gigapixel imagery as a medium for sharing geologic concepts." *GSA Northeastern Annual Meeting, Lancaster, PA USA, Abstract #15-4*.

Sargent, R, C. Bartley, P. Dille, J. Keller, I. Nourbackhsh, and R. LeGrand. 2010. "Timelapse GigaPan: Capturing, sharing and exploring timelapse gigapixel imagery." *Fine International Conference on Gigapixel Imaging for Science, Carnegie Mellon University, Pittsburgh, PA USA, Paper 22.*

Schoen, J. and R.D. Stevenson. 2010. "Uses of Gigapan technology in formal and informal environmental education." *Proceedings of the Fine International Conference on Gigapixel Imaging for Science, Carnegie Mellon University, Pittsburgh, PA USA*.

Sisk, M. 2010. "Three-dimensional GigaPan views of archeological sites and artifacts: examples from the Paleolithic of southwest France." *Fine International Conference on Gigapixel Imaging for Science, Carnegie Mellon University, Pittsburgh, PA USA, Paper 20*.

Steullet, A., J.L. Piatek, and M.C. Wizevich. 2010. "Using high-resolution panoramas of the geology of the western U.S. to illustrate concepts in introductory geoscience courses." *GSA Northeastern and Southeastern Joint Annual Meeting, Baltimore, MD USA, Abstract #38-7.*

Stimpson, I., R. Gertisser, M. Montenari, and B. O'Driscoll. 2010. "Multi-scale geological outcrop visualisation: using GigaPan and Photosynth in fieldwork-related geology teaching." *EGU General Assembly, Vienna, Austria,* pp. 4702.

Valentino, J.D., D.W. Valentino, A.P. O'Hara,and H. Valentino. 2011. "Effects of Adirondack Basement Uplift on Joints and Fault Development in the Appalachian Basin Margin, New York." *NYSGA Field Trip, A-1.*

Valentino, D.W., J.R. Chiarenzelli, E.M. Hewitt, and J.D. Valentino. 2012. "Applications of water-based magnetic gradiometry to assess the geometry and displacement for concealed faults in the southern Adirondack Mountains, New York, U.S.A." *J. Appl. Geophys.* 76: 109-126.

VanEyl-Godin, K. and K. VanZytveld. 2015. "Photographic measurement of sand movement in gigapixel panoramas reveals short term variability in geomorphologically similar Lake Michigan dunes." *14th Annual Celebration of Undergraduate Research and Creative Performance, Hope College, Holland MI USA, Paper 33.*

Wallach, J. 2002. "The presence, characteristics and earthquake implications of the St. Lawrence fault zone within and near Lake Ontario," *Tectonophysics* 353: 45-74.

Weinell, M., R.J. Lee, and A.H. Graettinger. 2017. "The mystery of maars: Characterization of maar-diatreme deposits at Hopi Buttes Volcanic Field (AZ) using GigaPan and thermal infrared techniques." *GSA Northeastern Annual Meeting, Pittsburgh, PA USA, Abstract #55-1.*

Wizevich, M. and J.L. Piatek. 2013. "Learning on ice: Development of online learning resources for glacial geology using GigaPan technology." *GSA Northeastern Annual Meeting, Denver, CO USA, Abstract #11-7.*

Yang, X. and H. Gao. 2018. "Full-wave seismic tomography in the northeastern United States: new insights into the uplift mechanism of the Adirondack mountains, *Geophys. Res. Lett.* 45: 1-9

"Silhouette and Layers" // Norman Ridge. Vermontville, NY